

Scotopic Contour Deformation Detection Reveals Early Rod Dysfunction in Age-Related Macular Degeneration With and Without Reticular Pseudodrusen

Brett G. Jeffrey,¹ Oliver J. Flynn,¹ Laryssa A. Huryh,¹ Maximilian Pfau,^{1,2} and Catherine A. Cukras¹

¹National Eye Institute, National Institutes of Health, Bethesda, Maryland, United States

²University of Bonn, Bonn, Germany

Correspondence: Catherine Cukras, Unit on Clinical Investigation of Retinal disease, National Eye Institute/NIH, Bethesda MD 20892, USA; cukrasc@nei.nih.gov.

Received: December 10, 2021

Accepted: April 26, 2022

Published: June 24, 2022

Citation: Jeffrey BG, Flynn OJ, Huryh LA, Pfau M, Cukras CA. Scotopic contour deformation detection reveals early rod dysfunction in age-related macular degeneration with and without reticular pseudodrusen. *Invest Ophthalmol Vis Sci.* 2022;63(6):23. <https://doi.org/10.1167/iops.63.6.23>

PURPOSE. The purpose of this study was to investigate scotopic contour deformation detection (sCDD), and its structural determinants, in participants with intermediate age-related macular degeneration (iAMD) with or without reticular pseudodrusen (RPD).

METHODS. Forty-one participants (aged 58–89 years), including 9 with iAMD and RPD, 16 with iAMD only, and 16 controls, underwent functional testing. The sCDD was evaluated with radial frequency arcs presented at 4 loci: ± 4 degrees and 8 degrees vertical eccentricity. Scotopic thresholds and dark adaptation (DA) were measured at the same loci. Retinal layers of spectral domain optical coherence tomography (SD-OCT) volume scans were segmented. To establish the concurrent validity of the functional test, we evaluated the fraction of variability in sCDD thresholds explained by SD-OCT data.

RESULTS. The iAMD group had significantly worse sCDD thresholds compared with controls (8 degrees inferior retina: $P = 0.004$ and the 4 degrees loci: $P < 0.02$ for both). Elevated sCDD thresholds were observed in iAMD and RPD eyes at loci with normal scotopic thresholds; the opposite was rarely encountered. Elevated sCDD thresholds were also observed in iAMD eyes with normal DA. Elevated sCDD thresholds were associated with increased age and presence of late AMD in the fellow eye. The optimal machine learning model predicted 16% of variability (cross-validated R^2) in sCDD thresholds at 8 degrees.

DISCUSSION. A novel scotopic contour deformation task can provide unique information about rod dysfunction in participants with iAMD and RPD not observed with structural and other functional assessments. Rod dysfunction observed with scotopic contour deformation testing was associated with factors linked to risk of AMD progression.

Keywords: shape discrimination, contour deformation, dark adaptation, scotopic thresholds, age-related macular degeneration, subretinal drusenoid deposits, reticular pseudodrusen

The impacts of visual symptoms from the perspective of the patient with age-related macular degeneration (AMD) have been analyzed using a range of patient reported outcome measures (PROMs). These include the Low Luminance Questionnaire (LLQ),¹ the Night Vision Questionnaire (NVQ-10),² and the Rasch-analyzed Impact of Visual Impairment questionnaire (IVI-28).^{3,4} Visual symptoms reported by people with AMD include difficulty with moving under low luminance conditions, driving at night, and adjusting to changes in lighting.^{1–3,5} PROM subscale scores (e.g. night driving) are significantly associated with rod-mediated parameters of dark adaptation,^{1,6,7} scotopic retinal sensitivity,⁵ and low-luminance visual acuity deficit.⁸ The reduction in rod-mediated function and associated night vision difficulties in patients with AMD are consistent with histological findings showing preferential loss of rods over cones in most donor eyes of patients with AMD.^{9,10}

In patients with AMD and reticular pseudodrusen (RPD), rod-mediated function is altered along a steep gradient

across the central retina. Specifically, dark adaptation is slowed, and scotopic sensitivity reduced most dramatically in points close to the fovea (4–6 degrees), with lesser dysfunction at loci farther from the fovea (≥ 8 degrees) — a pattern not seen in healthy aged eyes.^{7,11–16} However, there is large variation in rod-mediated function, both across and within AMD severity groups.^{14,15,17–19} Additionally, many patients with early to intermediate AMD have rod-mediated function within the normal range and show minimal progression of dark adaptation or scotopic sensitivity deficit over follow-up periods ranging from one^{20–22} to 4 years.⁷ A more sensitive test capable of detecting the earliest changes in rod function would be beneficial to the study of AMD.

Although rods appear to be affected early in the disease process, adaptive optics (AOs) enhanced imaging shows disruption of the cone photoreceptor mosaic and a moderate reduction in cone density over drusen.^{25–26} Photoreceptors form the front end of the neural visual system, and the

visual process begins by sampling of the retinal image by the photoreceptor mosaic.²⁷ Therefore, cortically mediated vision tasks, such as hyperacuity,^{28,29} would be predicted to be sensitive to disruption of the cone mosaic. Hyperacuity forms the basis of several tests that use shape discrimination or Vernier alignment to assess AMD severity^{27,30–33} and monitor progression of wet AMD.^{34,35} However, these tests are photopic and, therefore, measure the health of only cone photoreceptors.

We posited that modification of the shape discrimination test to assess spatial variation in rod function may prove beneficial in detecting early changes of the rod photoreceptor mosaic noted in histological studies of AMD eyes.⁹ We recently developed a rod-mediated, contour deformation detection test.³⁶ For this test, the task for the dark-adapted participant is to detect small deviations from circularity in an arc-shaped stimulus.³⁶ The scotopic contour deformation detection (sCDD) test relies on a wide area of healthy rod photoreceptors to allow for the integration of curvature information. We hypothesized that any change in the rod photoreceptor population (e.g. morphology, abundance, and/or rod displacement) due to AMD would elevate sCDD thresholds, even when rod loss is not great enough to decrease scotopic sensitivity. Here, we investigate sCDD in patients with intermediate AMD (iAMD) with or without RPD and its relationship to the locus-specific retinal structure.

METHODS

Study Population

Participants included 25 adults with iAMD or RPD aged (mean \pm SD) 72.8 ± 7.8 years old and 16 healthy volunteers aged 67.4 ± 6.6 years old. Participants with AMD and RPD were recruited from the eye clinic at the National Eye Institute, National Institutes of Health (NIH, Bethesda, MD, USA). Healthy volunteers were recruited from the Clinical Research Volunteer Program at the National Institutes of Health Clinical Center or responded to the posting on ClinicalTrials.gov (identifier: NCT02617966). The study was approved by the Institutional Review Board of NIH, is Health Insurance Portability and Accountability Act (HIPAA) compliant, and adhered to the Declaration of Helsinki. All participants provided informed consent.

Based on clinical examination and medical records, participants were excluded for (1) other ocular or macular diseases (e.g. glaucoma or diabetic retinopathy), (2) cataract surgery within the past 3 months before enrollment, (3) history of vitamin A deficiency, (4) high intake of vitamin A palmitate supplement ($\geq 10,000$ international units per day), and (5) active liver disease or history of liver disease.

Ophthalmic Examination and Imaging

Participants had a complete ophthalmic examination, including best corrected visual acuity (BCVA), intra-ocular pressure, slit lamp examination, and dilated fundus examination. Presence of AMD features (drusen, pigmentary change, pigment epithelial detachment, choroidal neovascularization [CNV], and central geographic atrophy) and other ocular findings (e.g. lens status and phakic status) were documented. Color-fundus photographs were captured with the TRC-50DX retinal camera (Topcon Corp., Tokyo, Japan). Fundus autofluorescence, infrared reflectance, and

spectral-domain optical coherence tomography (SD-OCT) were acquired with the Heidelberg Spectralis (Heidelberg Engineering, Heidelberg, Germany). SD-OCT volume scans covering at least a $20^\circ \times 15^\circ$ rectangle centered over the fovea, were available for structure-function analysis.

Study Eye Categorization

Participants were separated into groups based on their fundus appearance from color fundus photographs. We based our groups on the presence of large drusen ($>125 \mu\text{m}$ in diameter) in color images. Participants in the control group lacked large drusen or pigment changes whereas eyes in the iAMD group had drusen $>125 \mu\text{m}$ with or without pigmentary changes. Patients with iAMD were also screened for the presence of RPD based on grading both fundus autofluorescence and infrared reflectance images in conjunction with OCT review.¹⁹ For the purpose of this study, eyes with intermediate AMD and RPD will be referred to as RPD, whereas eyes with iAMD but without RPD will be referred to as iAMD.

Measurement and Analysis of sCDD Thresholds

The sCDD task we used in this study is based on a radial frequency (RF) pattern (Fig. 1). The testing apparatus, procedure, and basis of the task have been described in detail previously.³⁶ The radial frequency pattern is defined as a ring with a luminance profile modulated by a fourth-derivative (D4) Gaussian (see Fig. 1A) and a radius deformed by a sine wave (see Fig. 1B).³⁷ The radial frequency pattern is described by: radius (degrees of the visual angle) from the center of the ring to the D4 peak; radial frequency (the number of sine wave cycles per 360 degrees); spatial frequency (cycles per degree [CPD] of visual angle, which defines the thickness of the D4 Gaussian); contrast; and deformation amplitude, defined by the height of the

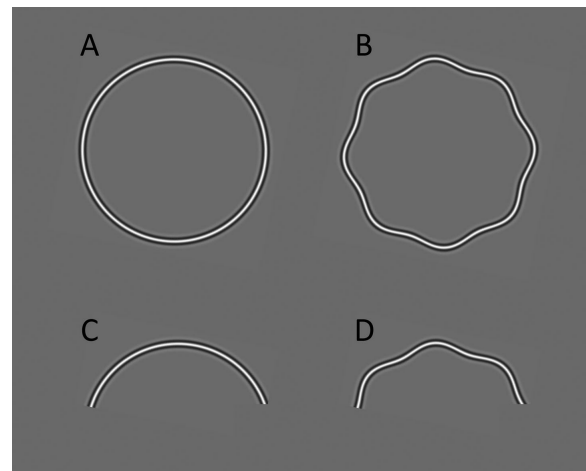


FIGURE 1. Examples of radial frequency (RF) patterns. (A) A nondeformed RF ring with a luminance profile defined by a fourth-derivative Gaussian. (B) An RF pattern with a radial frequency of eight, meaning that the ring is deformed by eight cycles of a sine wave. (C, D) For this stimulus with a radius of 4 degrees, part of the ring is occluded leaving three of the eight cycles visible (see text for rationale of stimulus occlusion). Other stimulus parameters; spatial frequency = 2 cycles per degree, contrast = 100% and maximum luminance = 0.002 cd/m^2 .

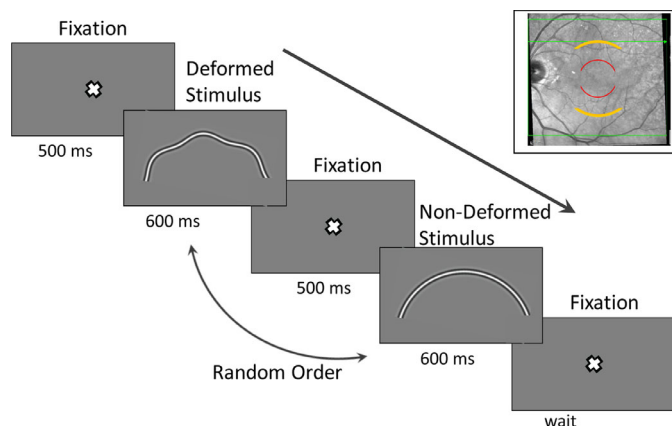


FIGURE 2. The trial sequence. A fixation cross was displayed for 500 ms, followed by either a deformed or nondeformed RF arc for 600 ms, followed by the fixation cross, followed by the remaining stimulus and returning to a fixation cross. A tone indicated a participant's response. *Inset:* Arcs show the size and relative position of nondeformed arcs at 4 degrees (red) and 8 degrees (yellow) eccentricity projected on the retina. The yellow arcs approximate the actual arc size.

deforming sine wave as a proportion of the mean radius (on a scale from 0 to 1).

For the current study, part of the ring was occluded, leaving three visible cycles (Figs. 1C, 1D). The reason for this partial occlusion is that the visual system, under dark adapted conditions, uses curvature information across only three cycles of RF modulation to make a judgment of circularity.³⁶ This finding held for all radii and radial frequencies tested.³⁶

The sCDD thresholds were measured at 4 eccentricities, with radius from the center of the ring to the fovea set at 4 degrees and 8 degrees and stimuli presented in both inferior and superior hemispheres (Fig. 2). The choice for these stimulus locations was based on a number of considerations. First, rod-mediated function is altered along a gradient across the macula in patients with AMD,^{13–15} with greater dysfunction in the superior retina, particularly in patients with RPD.¹⁵ Second, sCDD thresholds from healthy volunteers are not dependent on the radius of the stimulus between 2 degrees and 8 degrees retinal eccentricity.³⁶ Therefore, we chose the four stimulus loci to evaluate whether sCDD thresholds varied with eccentricity and/or hemisphere in patients with iAMD and RPD. Note that all location descriptors in this paper refer to retinal space (i.e. not visual field space). The stimulus at 4 degrees was a 3/8 RF arc (3 visible from 8 radial cycles; see Fig. 1). At 8 degrees, the stimulus was a 3/16 RF arc (3 visible from 16 radial cycles). These combinations of radii and radial frequencies ensure an equivalent amount of curvature information at each eccentricity as measured by circular contour frequency (CCF).^{36,38} Circular contour frequency (units of cycles per contour length degree [cycles/cl-deg]) is a measure of the physical length on the retina of one cycle of modulation around the circumference of a radial frequency pattern. For both stimulus conditions used in the current study, circular contour frequency was 0.32 cycles/cl-deg (i.e. each cycle subtended 3.14 degrees on the retina and 9.4 degrees for the 3 visible cycles) which produces the best sCDD thresholds in healthy volunteers.³⁶ For all tests, the following stimulus parameters were fixed: contrast = 100%, spatial frequency = 2 cycles per degree, and maximum luminance = 0.002 cd/m². To achieve this luminance, the monitor was calibrated by setting the maximum luminance of the display

to 1 cd/m² and placing 3 neutral density filters (0.9121, 0.9410, and 0.8452 log unit reductions) in front of the monitor.³⁶

Prior to testing, participants were asked to sit in the dark for 30 minutes. The sCDD threshold was measured from one eye using a two-alternative temporal forced choice discrimination task: pairs of smooth and deformed RF pattern arcs were presented in random order (see Fig. 2). Observers selected which of the two arcs was “bumpy” or deformed. The sCDD threshold (arcsec) was measured as the smallest noticeable difference between the radius of the smooth pattern (i.e. perfectly circular arc) and the radius at the peak of the deforming sine wave in the radial frequency pattern. The test followed an accelerated stochastic approximation staircase procedure³⁹ with 12 reversals. The sCDD threshold was the deformation amplitude presented on the final trial, converted to arcsec.⁴⁰ The log of the sCDD thresholds were normally distributed and used hereafter. At each test locus, threshold was the average of estimates from two staircases.

The inset in Figure 2 shows the size and relative position of non-deformed arcs at 4 degrees (red) and 8 degrees (yellow) projected on the retina. Note that only one of the four locations (e.g. 4 degrees superior) was ever tested during a trial sequence.

To familiarize the participant with testing, a practice session using a full eight radial frequency ring, presented photopically, was completed prior to dark adaptation and scotopic testing. All testing was conducted in a dark room with no light sources other than the stimulus monitor. Observers sat 1.2 meters from the monitor with an eye patch over the untested eye and trial lenses to correct for refractive error over the tested eye.

Measurement and Analysis of Scotopic Threshold and Dark Adaptation

Scotopic light detection threshold (hereafter, called scotopic threshold) and dark adaptation were measured using a Medmont Dark Adapted Chromatic (DAC) perimeter (Medmont, Nunawading, VIC, Australia). The test protocols and analysis procedures for these two tasks have been described in detail previously.¹⁵ Briefly, following pupil

dilation and 30 minutes in the dark, monocular scotopic thresholds were measured in response to a red (dominant wavelength = 625 nm) and cyan (dominant wavelength = 500 nm) stimuli at 4 degrees and 8 degrees inferior and superior to the fovea. The principles of the two color perimetry were used to determine whether scotopic thresholds were mediated by rods and/or cones at each loci.⁴¹⁻⁴³ Scotopic thresholds were expressed in absolute terms of light (scotopic log candela/meter² [sc cd/m²]).

After scotopic thresholds were measured, participants were exposed to a full-field light for 5 minutes to bleach approximately 30% of the rhodopsin. Dark adaptation was then measured monocularly at the same four retinal loci from scotopic threshold testing. Immediately after the bleach, thresholds were measured at the four loci. Testing of thresholds at each time point took less than 1 minute. After each round of testing, rest intervals were provided (30 seconds for the first 6 minutes after bleaching, and 60 seconds thereafter) and total recording time was 30 to 45 minutes; testing was terminated if a plateau in dark adaptation was evident across all points. Data were fit to a curvilinear model of dark adaptation⁴⁴ and the time to reach a criterion threshold of $-3.1 \log \text{cd/m}^2$ (Rod Intercept Time [RIT]) was calculated.

Structure Measurement of the Retina/RPE Complex

Feature Extraction. SD-OCT volume scans for the participants with iAMD and RPD and six controls were

segmented using a previously validated convolutional neural network.⁴⁵ Based on these segmentations, thickness maps (Fig. 3A) and mean intensity maps (Fig. 3B) were generated for the following layers: inner retina = from the internal limiting membrane (ILM) to the outer plexiform layer (OPL)/outer nuclear layer (ONL) boundary; Henle's fiber layer plus ONL (HFL + ONL) = from the OPL/ONL boundary to the external limiting membrane (ELM); photoreceptor inner segments (IS) = from the ELM to the ellipsoid zone (EZ) peak intensity; photoreceptor outer segments (OS) = from the EZ peak intensity to the inner boundary of the retinal pigment epithelium-deposit complex (RPEDC); the RPEDC, and the choroid (CHO). The RPEDC inner boundary was the next hyper-reflective structure outside to the EZ (or in the absence of EZ, the next hyper-reflective structure outside to the ELM). This boundary could represent either the inner boundary of the RPE (with or without underlying drusen), or the inner boundary of the RPD. The RPEDC outer boundary was Bruch's membrane. Thus, the RPEDC encompassed RPD, the RPE, and drusen putative basal laminar deposits, as well as Bruch's membrane.

The mean intensity maps constitute a 2D (en face) projection showing the mean reflectivity for a given layer along each A-scan (see Fig. 3B).

A custom ImageJ plugin was used to extract the means and standard deviations of the layer thicknesses and reflectivity values for regions-of-interest matching the stimulus positions and areas (see Fig. 3A). To compensate for variation in SD-OCT scan brightness, mean values of the mean-intensity projections were normalized relative to the average of the mean-intensity projection of the inner retina. We chose

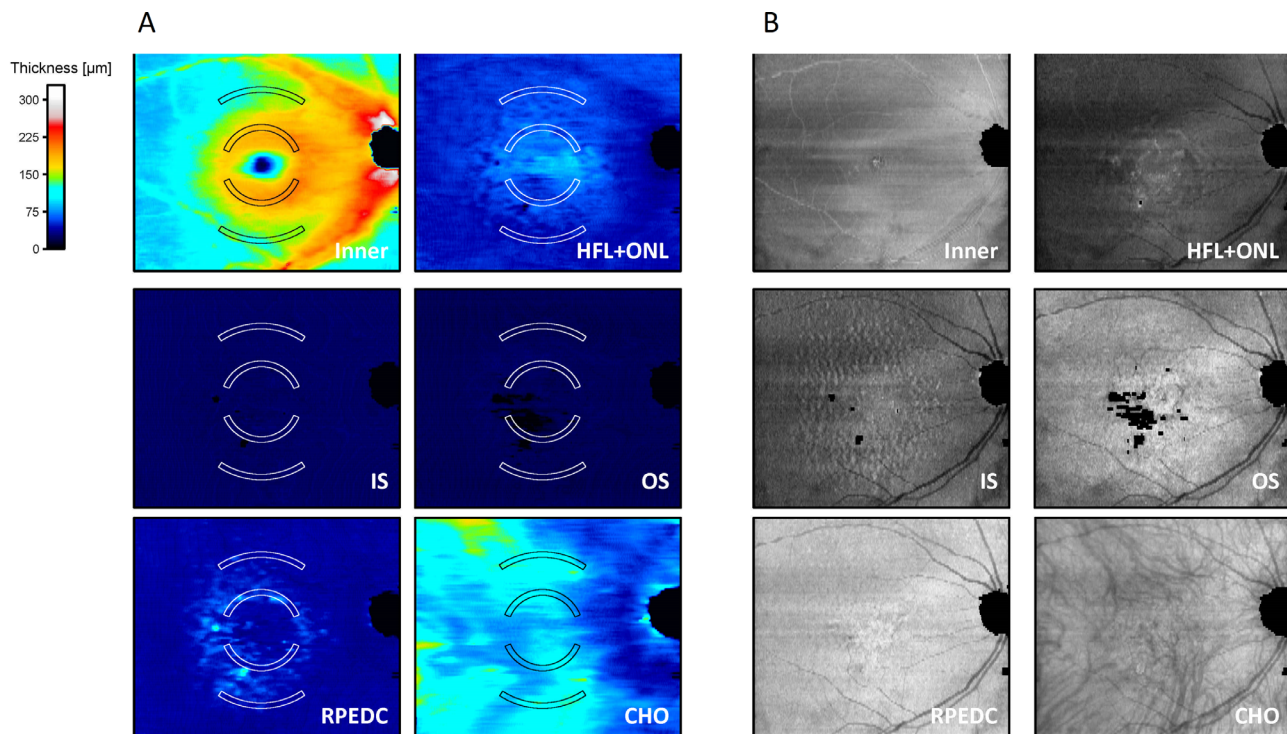


FIGURE 3. Feature extraction. Following segmentation of the SD-OCT data, thickness maps (shown as pseudo color maps (A)) and mean intensity projections (B) were generated for each layer. Subsequently, the average and standard deviation of the thickness for each layer were extracted at each stimulus position (*white contours* in pseudo color maps in A). Average and standard deviation of the mean intensity projection at each stimulus position for each layer were similarly calculated (B: stimulus contours not shown). Abbreviations: inner, inner retina; HFL+ ONL, Henle's fiber layer plus outer nuclear layer; IS, photoreceptor inner segments; OS, photoreceptor outer segments; RPEDC, retinal pigment epithelium-deposit complex; CHO, choroid. See Feature Extraction in Methods for layer definitions.

the inner retina for normalization, as we reasoned this layer was the most unaffected in our population.

Structure-Function Analysis. The structure-function analysis was performed separately for the loci at 8 degrees and 4 degrees with the sCDD thresholds as the dependent variable. Four sets of potentially predictive features were evaluated as explanatory variables:

- *Null model:* No predictive features, “prediction” constitutes mean of the sCDD thresholds in the respective training set (n-1 subjects)
- *Feature set 1:* Only the vertical position (superior/inferior retina) and subgroup (healthy volunteer, participants with iAMD, and RPD)
- *Feature set 2:* Addition of retinal layer thickness values (mean and standard deviation)
- *Feature set 3:* Addition of retinal reflectivity values (mean and standard deviation)

Three learning algorithms were considered: least absolute shrinkage and selection operator (LASSO) regression, principal component regression (PCR), and random forest regression.⁴⁶ These algorithms were chosen based on their ability to handle collinear predictors (i.e. typically thinning of HFL + ONL, IS, and OS co-occur in a given eye). Leave-one-out cross-validation (i.e. iteratively fitting the model to the data of n-1 subjects and then testing it on the data of the one held-out subject) was applied to tune the respective model parameters (lambda for LASSO, number of components for PCR, and mtry for random forest regression) and to evaluate the model performance in terms of the mean absolute error (MAE) between the observed and predicted sCDD thresholds.

RESULTS

Forty-one participants (26 women) were recruited: 16 healthy volunteers with a median age (range) of 67 years (range = 59–81), 16 participants with iAMD: 73 years (range = 58–85), and 9 participants with RPD: 70 years (range = 63–89). There was no significant age difference between groups (ANOVA: $P = 0.14$). Among healthy volunteers, study eyes had a BCVA of 20/20 or better and all participants with iAMD or RPD had a BCVA of 20/32 or better. Participants self-identified as White ($N = 34$), Asian ($N = 5$), or Black ($N = 1$); one participant chose not to self-identify with a race.

Figure 4 shows mean sCDD thresholds, scotopic thresholds, and RIT plotted as a function of retinal eccentricity for each AMD group. A 2-way ANOVA revealed no statistically significant interaction between the effects of retinal eccentricity and the AMD group on sCDD thresholds ($F(6, 117) = 1.8, P = 0.114$). However, main effects analysis showed that both retinal eccentricity ($P = 0.001$) and AMD group ($P = 0.016$) had a significant effect on sCDD threshold. Post hoc analysis indicated that the iAMD group had significantly worse (i.e. elevated) sCDD thresholds relative to the control group at three of the four test loci (see Fig. 4A). Mean elevation in sCDD threshold was slightly higher at the 8 degrees inferior locus (0.289 log arcsec, $P = 0.004$) compared with mean elevation at the 4 degrees loci (inferior = 0.218 log arcsec, superior = 0.207 log arcsec, $P < 0.02$ for both). Test-retest variability ranged from 0.118 to 0.152 log arcsec across the 4 retinal loci.

When tested with a mixed effects analysis, there was no interaction between eccentricity and the AMD group for scotopic thresholds to the 505 nm stimulus ($F(6, 117) = 1.2, P = 0.306$). Main effects analysis indicated these scotopic thresholds varied with retinal eccentricity ($P = 0.001$) but not the AMD group ($P = 0.154$; see Fig. 4B). Similarly, scotopic thresholds to the 625 nm stimulus and difference thresholds (625–505 nm) varied with eccentricity ($P < 0.0001$ and $P = 0.043$, respectively) but not AMD severity (data not shown) and there was no interaction for either measure.

Figure 4C shows that RIT varied with the AMD group and retinal eccentricity (mixed effects analysis [$F(6, 99) = 11.83, P < 0.0001$] with main effects of the AMD group ($P < 0.0001$) and retinal eccentricity ($P < 0.0001$). The RPD group had significantly longer RIT compared with the controls for three of the four loci, with the superior retina more affected than the inferior retina (see Fig. 4C). The RPD group also had significantly longer RIT compared with the iAMD group for the two test loci from the superior retina (see Fig. 4C). The finding that RIT delay is most pronounced across the superior retina, particularly for the patients with RPD, stands in contrast to the effect of hemisphere on the sCDD thresholds. As noted above, the largest sCDD deficits were found for the loci from the inferior retina.

Figure 5 shows the relationship between sCDD thresholds and scotopic thresholds for the two AMD groups. At all four locations (see Fig. 5A–D), elevated sCDD thresholds could be observed in eyes with normal scotopic thresholds (blue shaded areas). In contrast, normal sCDD thresholds in conjunction with elevated scotopic thresholds were rarely observed (yellow shaded areas). The most pronounced change in sCDD was observed at the 8 degree inferior locus where 6 of 16 (38%) participants with iAMD (reddish-purple circles) and 3 of 9 (33%) participants with RPD (blue diamonds) had markedly elevated sCDD thresholds in the presence of normal scotopic thresholds (see Fig. 5C: blue shaded area). The sCDD thresholds for the 6 participants with iAMD were elevated above the upper limit of normal by a median of 0.288 log arcsec (94% increase). For the 3 participants with RPD, median sCDD threshold elevation was 0.271 log arcsec (87% increase). A similar pattern was observed at the 4 degree inferior test locus, but a fewer number of participants with normal scotopic thresholds had abnormal sCDD thresholds, and these participants had a less pronounced elevation in sCDD thresholds (iAMD: $N = 5$ [31%], 0.165 log arcsec [46% increase]; and RPD: $N = 1$ [11%]; elevation = 0.303 log arcsec). The sCDD was less affected in the superior retina. The sCDD thresholds were elevated across the 2 superior loci by a median of 0.129 log arcsec (35% increase) in the 3 participants with iAMD with normal scotopic thresholds and by 0.162 log arc (45%) for a single participant with RPD. All participants with elevated sCDD thresholds in Figure 5 panels A, B, and D were a subset of the participants with abnormal sCDD thresholds at the 8 degrees inferior locus (see Fig. 5C). At all four loci, the sCDD thresholds had low-to-moderate correlation with scotopic thresholds (Supplementary Fig. S1).

Figure 6 explores the relationship between sCDD threshold and dark adaptation, as measured from RIT. For the participants with iAMD, the association between RIT and sCDD thresholds broadly mirrors that described above. For example, at the 8 degrees and 4 degrees of the inferior loci, 4 (25%) and 3 (19%) participants with iAMD, respectively, had markedly elevated sCDD thresholds but normal RIT

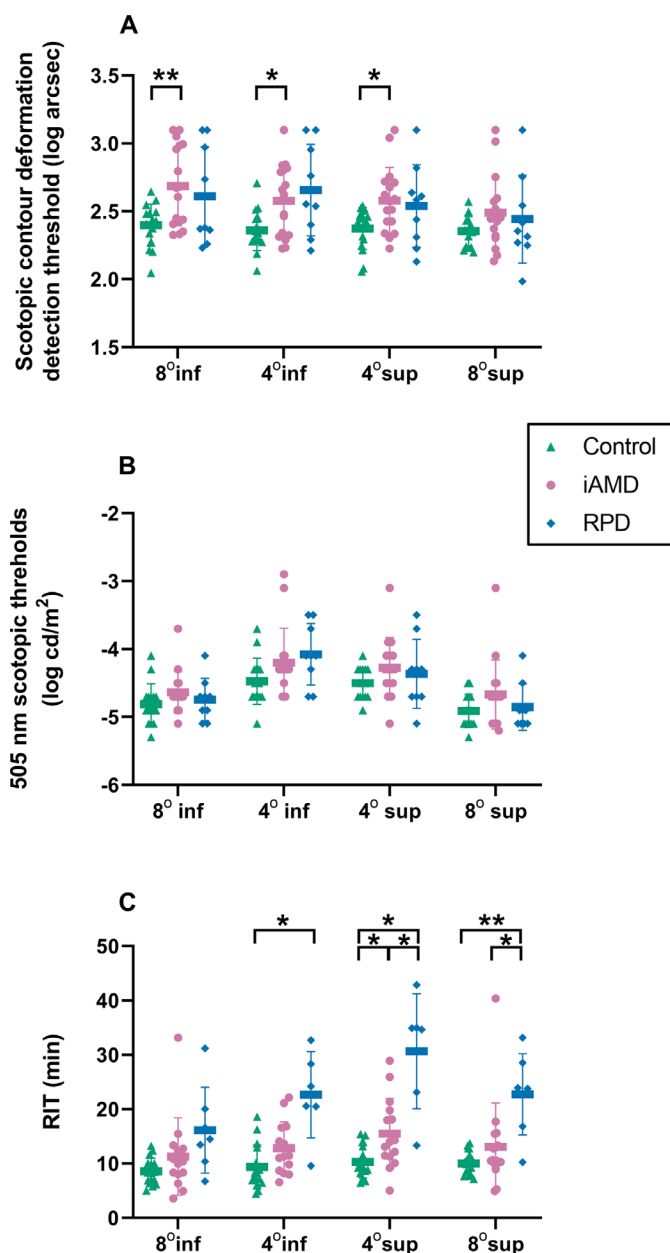


FIGURE 4. Scatter dot plots showing sCDD thresholds (A), scotopic thresholds to a 505 nm stimulus (B), and RIT (C) at each of the four retinal eccentricities tested. Post hoc comparisons: * $P < 0.05$; ** $P < 0.01$. Horizontal bars show means, vertical lines show standard deviations. Abbreviations: sCDD, scotopic contour deformation detection; inf, inferior; sup, superior; iAMD, intermediate age-related macular degeneration; RPD, reticular pseudodrusen; RIT, rod intercept time.

(see Figs. 5C, 5D: blue shaded areas); this subset of participants with iAMD also had normal scotopic thresholds. Dark adaptation was delayed in almost all participants with RPD. Notably, six of the eight participants with RPD (75%) with prolonged dark adaptation at the two test loci in the superior retina had normal sCDD thresholds at these same test locations (see Figs. 6A, 6B). In contrast, no patient in the RPD group had an elevated sCDD threshold combined with normal RIT. The sCDD thresholds were moderately correlated with RIT only at the 4 degree inferior locus ($P = 0.02$, $R = 0.5$); these two parameters were not correlated at the other test loci (Supplementary Fig. S2).

We investigated whether clinical differences between participants might account for elevated sCDD thresholds in some participants but not others. The following clinical/ocular characteristics were compared: age, BCVA, pseudophakic status, and the presence of cataract, epiretinal membranes (ERM) or late AMD (geographic atrophy [GA] or choroidal neovascularization) in the fellow eye. Participants with elevated sCDD thresholds were older for both the iAMD ($P = 0.026$) and the RPD ($P < 0.001$) groups. The sCDD thresholds did not vary with age in the control group (Supplementary Fig. S3) indicating that aging alone did not account for the higher elevated sCDD thresholds

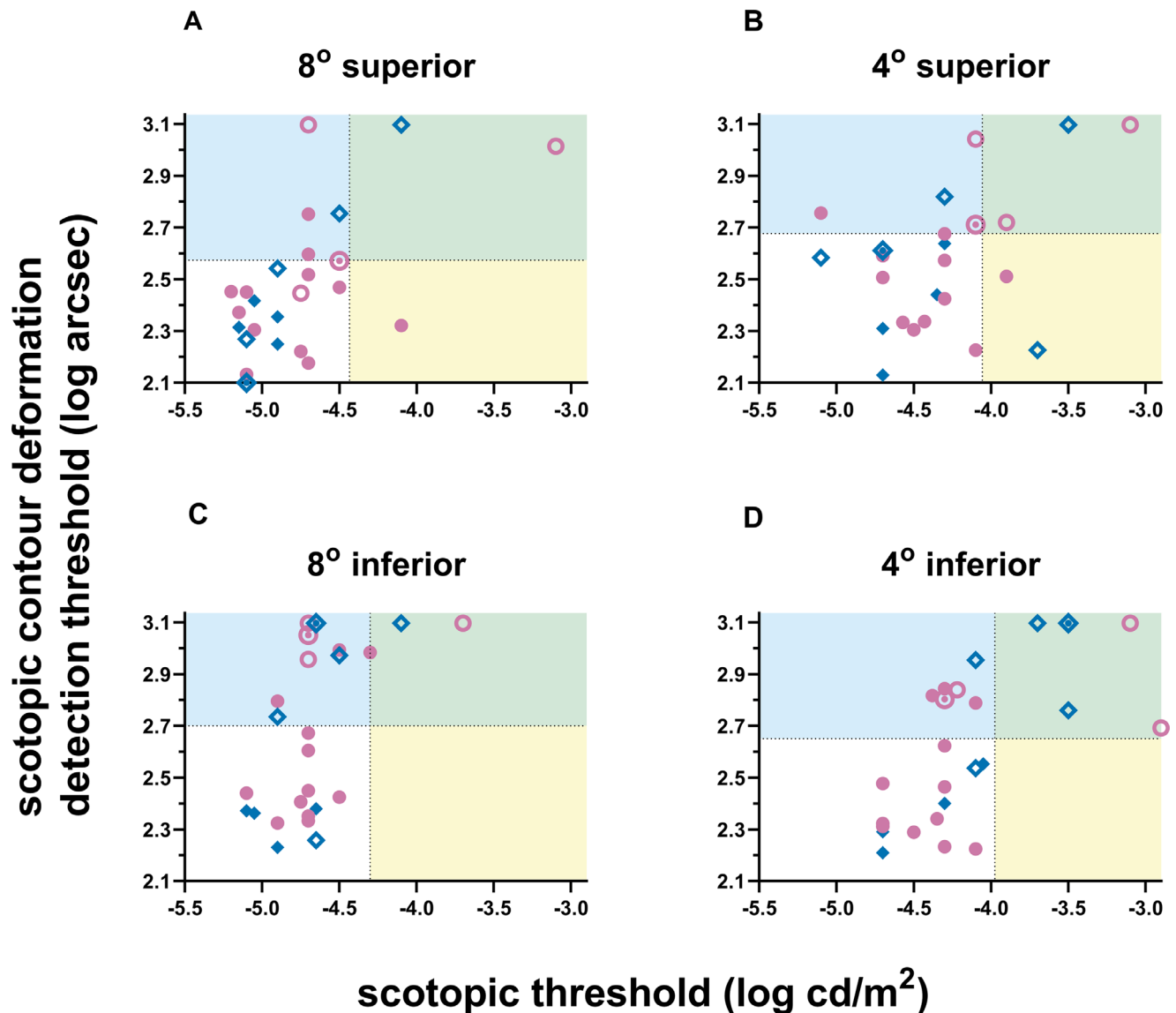


FIGURE 5. The sCDD thresholds for the iAMD (reddish purple symbols) and RPD (blue symbols) plotted as a function of scotopic thresholds at each of the four test loci. Each panel is divided into four sectors; the white area indicates normal sCDD and scotopic thresholds; the other three sectors indicate elevated sCDD thresholds (blue), elevated scotopic thresholds (yellow), or both thresholds elevated (green). Open symbols: Participants with late AMD in the non-tested eye. Open symbols with dots: Participants with visually significant cataracts.

in the iAMD and RPD groups. All participants with iAMD and four of five participants with RPD with late AMD in the fellow eye, had elevated sCDD thresholds in the inferior retina (see Fig. 5: open symbols). The two participants with visually significant cataracts also had elevated sCDD thresholds in the inferior retina (see Fig. 5: open symbols with dots). Three RPD participants had ERM that were not visually significant; no participants with iAMD had ERM. Lens status (natural, pseudophakia, and early cataract [nuclear category 1]) was not different between those participants with elevated and normal sCDD thresholds.

We sought to determine whether structural changes in the retina/RPE complex could explain elevations in sCDD thresholds. At 4 degrees eccentricity, the sCDD thresholds could only be predicted to a limited extent (Table 1). The best model (random forest regression with feature-

set 2) predicted sCDD thresholds with a cross-validated MAE (95% confidence interval [CI]) of 224.8 arcsec (95% CI = 162.3, 287.2); a marginal improvement over the null model with an MAE of 238.4 arcsec (95% CI = 175.5, 301.2; see Table 1). This means that just (cross-validated R^2) 7.6% of the variability in sCDD thresholds at 4 degrees eccentricity could be explained by the selected imaging biomarker panel.

In contrast, sCDD thresholds at 8 degrees could be predicted more accurately from imaging biomarkers. The most accurate model (PCR with feature set 3) predicted the sCDD thresholds with a cross-validated MAE of 247.0 arcsec (95% CI = 180.8, 313.2) compared with the null model MAE of 292.5 arcsec (95% CI = 224.5, 360.5; Table 2). Accordingly, (cross-validated R^2) 15.9% of the variability in the sCDD thresholds at 8 degrees could be explained by imaging

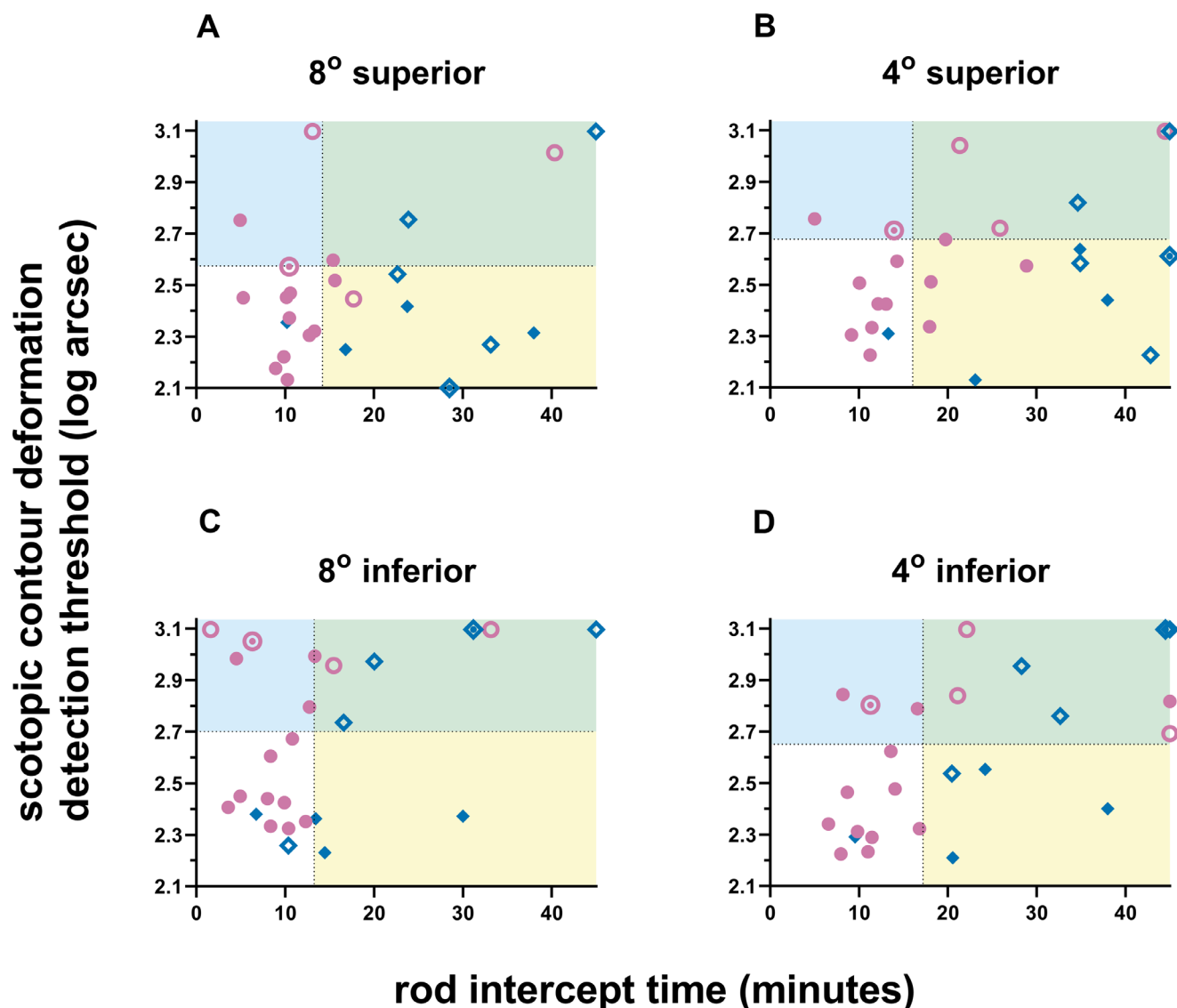


FIGURE 6. The sCDD thresholds for the iAMD (reddish purple symbols) and RPD (blue symbols) plotted as a function of rod intercept time (RIT) at each of the four test loci. As above, each panel is divided into four sectors; the white area indicates normal sCDD thresholds and normal RIT; the other three sectors indicate elevated sCDD thresholds (blue), prolonged RIT (yellow), or both elevated sCDD threshold and prolonged RIT (green). Open symbols: Participants with late AMD in the non-tested eye. Open symbols with dots: Participants with visually significant cataracts.

TABLE 1. Structure-Function Analysis at 4 Degrees Retinal Eccentricity

Eccentricity	Feature Set	Cross-Validated Mean Absolute Error (Estimate [95% CI]) in arcsec		
		LASSO Regression	PCR	Random Forest Regression
4 degrees	Null model		238.36 [175.5, 301.22]	
	Vertical position and subgroup	232.12 [168.45, 295.80]	231.22 [166.46, 295.98]	231.75 [166.87, 296.64]
	+ thickness maps	238.36 [175.50, 301.22]	246.62 [168.38, 324.87]	224.73 [162.28, 287.17]
	+ reflectivity maps	238.36 [175.50, 301.22]	242.65 [164.44, 320.85]	226.38 [164.85, 287.90]

Mean absolute error (MAE) between the observed and predicted sCDD threshold (in arcsec) at 4 degrees retinal eccentricity. The MAE for the best model for each feature set is highlighted in bold.

TABLE 2. Structure-Function Analysis at 8 Degrees Retinal Eccentricity

Eccentricity	Feature Set	Cross-Validated Mean Absolute Error (Estimate [95% CI]) in arcsec		
		LASSO Regression	PCR	Random Forest Regression
8 degrees	Null model		292.48 [224.45, 360.51]	
	Vertical position and subgroup	273.28 [201.80, 344.76]	279.62 [207.75, 351.49]	275.55 [202.36, 348.74]
	+ thickness maps	292.10 [223.57, 360.64]	264.59 [192.33, 336.86]	270.91 [198.07, 343.74]
	+ reflectivity maps	275.98 [204.45, 347.51]	246.99 [180.83, 313.16]	267.40 [195.50, 339.31]

Mean absolute error (MAE) between the observed and predicted sCDD threshold (in arcsec) at 8 degrees retinal eccentricity. The MAE for the best model for each feature set is highlighted in bold.

biomarkers. The three features, which showed the strongest correlation with the sCDD thresholds at 8 degrees were the normalized CHO mean intensity (Spearman's $\rho = 0.41$), CHO mean thickness ($\rho = -0.38$) and standard deviation of the IS thickness ($\rho = 0.33$).

DISCUSSION

The major finding from the current study is that a novel sCDD test reveals evidence of rod-mediated dysfunction in a subset of participants with iAMD with normal scotopic thresholds and normal dark adaptation. For participants with RPD, the sCDD also detected changes in rod-mediated function in a subset of the RPD group who had normal scotopic thresholds, but these participants with RPD also had delayed dark adaptation. A further important finding in this study is that sCDD is most affected in the iAMD and RPD groups across the inferior retina, and more so at the more eccentric of the two test loci. By contrast, delays in dark adaptation were greatest at the central loci and more so in the superior hemisphere of both the iAMD and RPD groups; results consistent with previous studies.^{14–16,22,47} Although this is a cross-sectional study, the observed data are compatible with a disease sequence of early abnormal contour deformation detection and subsequent elevation of scotopic thresholds. In contrast, the reverse pattern (normal sCDD thresholds, but abnormal scotopic thresholds), was not observable. Taken together, these results suggest that the sCDD test provides unique information about rod function in participants with iAMD and RPD and may prove useful in identifying early rod dysfunction in these participants. Early detection of rod dysfunction may be valuable given that elevated sCDDs were associated with age and advanced AMD in the non-test eye, factors that significantly increase the risk for the 5- and 10-year progression of AMD.⁴⁸

In healthy volunteers, the sCDD threshold measured with the partially occluded RF pattern used here is mediated by the amount of curvature information.³⁶ Curvature information is provided by both local cues (convex peaks of the stimulus)^{49,50} and the number of visible cycles (up to a maximum of 3).³⁶ By corollary, the increase in sCDD thresholds observed in the iAMD and RPD groups reflects a reduced ability of these participants to detect curvature. Disruption of the tightly packed polygonal photoreceptor mosaic in affected participants may account for the reduced ability to detect curvature. Histological studies of donor eyes with non-exudative AMD found a 30% reduction in photoreceptor density in the parafovea with a greater loss of rods than cones.^{9,10} This photoreceptor loss caused a marked alteration in the parafoveal photoreceptor mosaic evidenced by partially adjacent cones and sparse rod inner segments.⁹ Subsequent histology studies have further shown disruption of the photoreceptors over drusen and subretinal drusenoid

deposits (SDDs), the histologic correlate of RPD.^{51,52} These disruptions include thinning of the ONL, a sign of reduced photoreceptor numbers, as well as outer segment shortening and displacement of photoreceptors around the SDD. These histological findings have been further supported by subsequent AO-assisted imaging studies that revealed both decreased cone reflectivity and irregular variation in cone reflectivity over drusen and RPD.^{23–26} These changes in reflectivity could result from loss of cones and/or their outer segments or alterations in the orientation of receptors. These combined results provide strong evidence for variable disruption of the photoreceptor matrix in AMD and RPD, which likely accounts for the loss of curvature detection necessary for scotopic contour deformation detection. Such changes at the photoreceptor level are unlikely to be reflected by macroscopic structural changes within the retinal layers, which likely accounts for why our model analysis provided limited prediction of the sCDD thresholds.

Within the scotopic pathway of the retina, multiple rods converge onto a single rod bipolar cell (RBC); in turn, multiple RBCs converge onto a single AII amacrine cell.⁵³ Histological measurements of rod, RBC, and AII amacrine cell densities from postmortem eyes, indicate that scotopic acuity is predicted from the spatial resolution limit of the AII amacrine mosaic for retinal eccentricities less than 15 degrees.⁵³ Scotopic acuity ranges from 8 to 9 cyc/deg (i.e. 450–400 arcsec) over the retinal eccentricities tested in the current study. By comparison, for our control group, the average \pm SD sCDD thresholds were 246 ± 83 arcsec and 249 ± 75 arcsec for the 4 degrees and 8 degrees loci, respectively. Thus, in the absence of AMD, sCDD thresholds are better than scotopic acuity and, therefore, not limited by the AII cell mosaic. However, we cannot rule out disruption of the convergence within the rod pathway (e.g. due to retinal remodeling⁵⁴) as a potential cause for the elevation in sCDD thresholds in some patients with AMD.

Why then are scotopic thresholds less affected than scotopic sCDD thresholds in participants with AMD and RPD? Scotopic thresholds represent the limit of detection of luminance contrast. Such luminance thresholds improve proportionally with the size of the stimulus (complete spatial summation) up to a limit known as Ricco's area.⁵⁵ At 73 years of age (median of our participants), Ricco's area in the dark adapted eye is estimated to be 1.13 degrees², which corresponds to a stimulus of 1.2 degrees in diameter.⁵⁶ Given that Ricco's area for our patients is smaller in size than the Goldmann V stimulus (1.7 degrees diameter) used, scotopic thresholds would be predicted to worsen in direct proportion to the average rod loss in the stimulus area, but insensitive to small, localized defects. We reported the coefficient of repeatability (CoR) of scotopic thresholds to be 7.2 dB,⁵⁷ which corresponds to an 80% loss of rod sensitivity. Assuming that rod loss is proportional to outer segment

thinning,^{58,59} an 80% reduction in rod sensitivity would result from an approximately 55% loss of rod photoreceptors (i.e. reduced to 0.45 [45%] of rod numbers times 0.45 [45%] of OS length = 0.2 [20%] sensitivity). Therefore, a greater than 55% loss of rods over a large area (1.2 degrees or 350 μ m diameter), located within the test stimulus loci is required to significantly lower scotopic threshold. In contrast, even a small amount of rod loss would be expected to disrupt the tightly packed photoreceptor matrix and disrupt scotopic contour deformation detection.

There was a much less clear relationship between the sCDD deficit and the delayed dark adaptation, particularly for participants with RPD. For example, some patients with RPD with delayed dark adaptation did not show a loss of sCDD. Dark adaptation is a measure of the rate of resupply of retinoid to rod photoreceptors following exposure to an intense light that bleaches rhodopsin. In contrast, both sCDD and scotopic sensitivity reflect rod-mediated function in the dark-adapted eye. The results in the patients with RPD suggest that while retinoid resupply is delayed in most participants, once fully dark adapted, some participants have normal rod-mediated function.

Tahir et al.¹⁶ also used an arc stimulus but with a goal of studying dark adaptation kinetics in early AMD. Their stimulus comprised non-deformed arcs at eccentricities of 3 degrees and 5.5 degrees; these arcs would subtend 4.0 degrees and 7.2 degrees on the retina respectively. Although the stimuli in the current study are similar in eccentricity and extent to those used by Tahir et al.,¹⁶ the goals and psychophysical tasks of the two studies are very different. Tahir et al.¹⁶ set out to investigate cone function and its relation to rod abnormalities during dark adaptation. To this end, the sizes and locations of the arc stimuli were designed to be photopically matched (i.e. equal number of cones) but with 2.5 times the amount of rods in the outer arc. The psychophysical task in the Tahir et al.¹⁶ study was still one of detection, as used in perimetry and dark adaptation assessment. Because of spatial summation, retinal sensitivity to the nondeformed arc stimulus is mediated by the most sensitive subregion within the stimulus, not the aggregate sensitivity across the entire stimulus. In contrast, contour deformation detection to our radial deformation arcs depends on curvature information which includes integration across the entire three cycles of the arc.

A limitation of our study is the relatively small sample sizes for our groups. As such, the estimates of the number of participants with AMD/RPD for whom the sCDD task would detect early rod dysfunction when dark adaptation and/or scotopic thresholds are within the normal range are approximate. Testing in a larger number of participants is required to verify these results and longitudinal follow-up will provide further insight into the relationship between sCDD and the progression of AMD.

Acknowledgments

This work was presented at the annual meeting of the Association for Research in Vision and Ophthalmology, Vancouver BC, Canada, April 28 to May 2, 2019.

Supported by the Intramural Research Program of the National Institutes of Health, National Eye Institute, Bethesda, Maryland, USA.

Disclosure: **B.G. Jeffrey**, None; **O.J. Flynn**, None; **L.A. Huryn**, None; **M. Pfau**, None; **C.A. Cukras**, None

References

- Owsley C, McGwin G, Jr., Scilley K, Kallies K. Development of a questionnaire to assess vision problems under low luminance in age-related maculopathy. *Invest Ophthalmol Vis Sci.* 2006;47:528–535.
- Ying GS, Maguire MG, Liu C, Antoszyk AN. Night vision symptoms and progression of age-related macular degeneration in the Complications of Age-related Macular Degeneration Prevention Trial. *Ophthalmology.* 2008;115:1876–1882.
- McGuinness MB, Finger RP, Wu Z, et al. Properties of the Impact of Vision Impairment and Night Vision Questionnaires Among People With Intermediate Age-Related Macular Degeneration. *Transl Vis Sci Technol.* 2019;8:3.
- McGuinness MB, Finger RP, Wu Z, et al. Association between Patient-Reported Outcomes and Time to Late Age-Related Macular Degeneration in the Laser Intervention in Early Stages of Age-Related Macular Degeneration Study. *Ophthalmol Retina.* 2020;4(9):881–888.
- Scilley K, Jackson GR, Cideciyan AV, Maguire MG, Jacobson SG, Owsley C. Early age-related maculopathy and self-reported visual difficulty in daily life. *Ophthalmology.* 2002;109:1235–1242.
- Yazdanie M, Alvarez J, Agron E, et al. Decreased Visual Function Scores on a Low Luminance Questionnaire Is Associated with Impaired Dark Adaptation. *Ophthalmology.* 2017;124:1332–1339.
- Chen KG, Alvarez JA, Yazdanie M, et al. Longitudinal Study of Dark Adaptation as a Functional Outcome Measure for Age-Related Macular Degeneration. *Ophthalmology.* 2019;126:856–865.
- Wu Z, Guymer RH, Finger RP. Low luminance deficit and night vision symptoms in intermediate age-related macular degeneration. *Br J Ophthalmol.* 2015;100(3):395–398.
- Curcio CA, Medeiros NE, Millican CL. Photoreceptor loss in age-related macular degeneration. *Invest Ophthalmol Vis Sci.* 1996;37:1236–1249.
- Medeiros NE, Curcio CA. Preservation of ganglion cell layer neurons in age-related macular degeneration. *Invest Ophthalmol Vis Sci.* 2001;42:795–803.
- Sunness JS, Massof RW, Johnson MA, Finkelstein D, Fine SL. Peripheral retinal function in age-related macular degeneration. *Arch Ophthalmol.* 1985;103:811–816.
- Steinmetz RL, Haimovici R, Jubb C, Fitzke FW, Bird AC. Symptomatic abnormalities of dark adaptation in patients with age-related Bruch's membrane change. *Br J Ophthalmol.* 1993;77:549–554.
- Owsley C, Jackson GR, Cideciyan AV, et al. Psychophysical evidence for rod vulnerability in age-related macular degeneration. *Invest Ophthalmol Vis Sci.* 2000;41:267–273.
- Fraser RG, Tan R, Ayton LN, Caruso E, Guymer RH, Luu CD. Assessment of Retinotopic Rod Photoreceptor Function Using a Dark-Adapted Chromatic Perimeter in Intermediate Age-Related Macular Degeneration. *Invest Ophthalmol Vis Sci.* 2016;57:5436–5442.
- Flynn OJ, Cukras CA, Jeffrey BG. Characterization of Rod Function Phenotypes Across a Range of Age-Related Macular Degeneration Severities and Subretinal Drusenoid Deposits. *Invest Ophthalmol Vis Sci.* 2018;59:2411–2421.
- Tahir HJ, Rodrigo-Diaz E, Parry NRA, et al. Slowed Dark Adaptation in Early AMD: Dual Stimulus Reveals Scotopic and Photopic Abnormalities. *Invest Ophthalmol Vis Sci.* 2018;59:AMD202–AMD210.
- Owsley C, McGwin G, Jr., Jackson GR, Kallies K, Clark M. Cone- and rod-mediated dark adaptation impairment in age-related maculopathy. *Ophthalmology.* 2007;114:1728–1735.
- Dimitrov PN, Robman LD, Varsamidis M, et al. Visual function tests as potential biomarkers in age-related

- macular degeneration. *Invest Ophthalmol Vis Sci*. 2011;52:9457–9469.
19. Flamendorf J, Agron E, Wong WT, et al. Impairments in Dark Adaptation Are Associated with Age-Related Macular Degeneration Severity and Reticular Pseudodrusen. *Ophthalmology*. 2015;122:2053–2062.
 20. Jackson GR, Clark ME, Scott IU, Walter LE, Quillen DA, Brigell MG. Twelve-month natural history of dark adaptation in patients with AMD. *Optom Vis Sci: Official Publication of the American Academy of Optometry*. 2014;91:925–931.
 21. Nguyen CT, Fraser RG, Tan R, et al. Longitudinal Changes in Retinotopic Rod Function in Intermediate Age-Related Macular Degeneration. *Invest Ophthalmol Vis Sci*. 2018;59:AMD19–AMD24.
 22. Tan RS, Guymer RH, Aung KZ, Caruso E, Luu CD. Longitudinal Assessment of Rod Function in Intermediate Age-Related Macular Degeneration With and Without Reticular Pseudodrusen. *Invest Ophthalmol Vis Sci*. 2019;60:1511–1518.
 23. Boretsky A, Khan F, Burnett G, et al. In vivo imaging of photoreceptor disruption associated with age-related macular degeneration: A pilot study. *Lasers in Surg Med*. 2012;44:603–610.
 24. Mrejen S, Sato T, Curcio CA, Spaide RF. Assessing the cone photoreceptor mosaic in eyes with pseudodrusen and soft drusen in vivo using adaptive optics imaging. *Ophthalmology*. 2014;121:545–551.
 25. Zhang Y, Wang X, Rivero EB, et al. Photoreceptor perturbation around subretinal drusenoid deposits as revealed by adaptive optics scanning laser ophthalmoscopy. *Am J Ophthalmol*. 2014;158:584–596.e581.
 26. Reumueller A, Schmidt-Erfurth U, Salas M, et al. Three-Dimensional Adaptive Optics-Assisted Visualization of Photoreceptors in Healthy and Pathologically Aged Eyes. *Invest Ophthalmol Vis Sci*. 2019;60:1144–1155.
 27. Wang YZ, Wilson E, Locke KG, Edwards AO. Shape discrimination in age-related macular degeneration. *Invest Ophthalmol Vis Sci*. 2002;43:2055–2062.
 28. Hu ML, Ayton LN, Jolly JK. The Clinical Use of Vernier Acuity: Resolution of the Visual Cortex Is More Than Meets the Eye. *Front Neurosci*. 2021;15:714843.
 29. Wilson HR, Wilkinson F. From orientations to objects: Configurational processing in the ventral stream. *J Vis*. 2015;15:4.
 30. Wang YZ, He YG, Mitzel G, Zhang S, Bartlett M. Handheld shape discrimination hyperacuity test on a mobile device for remote monitoring of visual function in maculopathy. *Invest Ophthalmol Vis Sci*. 2013;54:5497–5505.
 31. Faes L, Bodmer NS, Bachmann LM, Thiel MA, Schmid MK. Diagnostic accuracy of the Amsler grid and the preferential hyperacuity perimetry in the screening of patients with age-related macular degeneration: systematic review and meta-analysis. *Eye (London, England)*. 2014;28:788–796.
 32. Chen JS, Adelman RA. Hyperacuity Exam Screens for Choroidal Neovascularization in Age-Related Macular Degeneration on a Mobile Device. *Ophthalmic Surg Lasers Imaging Retina*. 2016;47:708–715.
 33. Schmid MK, Thiel MA, Lienhard K, Schlingemann RO, Faes L, Bachmann LM. Reliability and diagnostic performance of a novel mobile app for hyperacuity self-monitoring in patients with age-related macular degeneration. *Eye (London, England)*. 2019;33:1584–1589.
 34. Chew EY, Clemons TE, Bressler SB, et al. Randomized trial of a home monitoring system for early detection of choroidal neovascularization home monitoring of the Eye (HOME) study. *Ophthalmology*. 2014;121:535–544.
 35. Pitrelli Vazquez N, Harding SP, Heimann H, Czanner G, Knox PC. Radial shape discrimination testing for new-onset neovascular age-related macular degeneration in at-risk eyes. *PLoS One*. 2018;13:e0207342.
 36. Flynn OJ, Jeffrey BG. Scotopic contour and shape discrimination using radial frequency patterns. *J Vis*. 2019;19:1–12.
 37. Wilkinson F, Wilson HR, Habak C. Detection and recognition of radial frequency patterns. *Vis Res*. 1998;38:3555–3568.
 38. Jeffrey BG, Wang YZ, Birch EE. Circular contour frequency in shape discrimination. *Vis Res*. 2002;42:2773–2779.
 39. Faes L, Nollo G, Ravelli F, et al. Small-sample characterization of stochastic approximation staircases in forced-choice adaptive threshold estimation. *Percept Psychophys*. 2007;69:254–262.
 40. Swanson WH, Birch EE. Extracting thresholds from noisy psychophysical data. *Percept Psychophys*. 1992;51:409–422.
 41. Wald G, Zeavin BH. Rod and cone vision in retinitis pigmentosa. *Am J Ophthalmol*. 1956;42:253–269.
 42. Massof RW, Finkelstein D. Rod sensitivity relative to cone sensitivity in retinitis pigmentosa. *Invest Ophthalmol Vis Sci*. 1979;18:263–272.
 43. Jacobson SG, Voigt WJ, Parel JM, et al. Automated light- and dark-adapted perimetry for evaluating retinitis pigmentosa. *Ophthalmology*. 1986;93:1604–1611.
 44. Dimitrov PN, Guymer RH, Zele AJ, Anderson AJ, Vingrys AJ. Measuring rod and cone dynamics in age-related maculopathy. *Invest Ophthalmol Vis Sci*. 2008;49:55–65.
 45. Pfau M, von der Emde L, de Sisternes L, et al. Progression of Photoreceptor Degeneration in Geographic Atrophy Secondary to Age-related Macular Degeneration. *JAMA Ophthalmol*. 2020;138:1026–1034.
 46. Hastie T, Tibshirani R, Friedman J. *The Elements of Statistical Learning – Data Mining, Inference and Prediction*. 2nd ed. New York, NY: Springer; 2009.
 47. Luu CD, Tan R, Caruso E, Fletcher EL, Lamb TD, Guymer RH. Topographic Rod Recovery Profiles after a Prolonged Dark Adaptation in Subjects with Reticular Pseudodrusen. *Ophthalmol Retina*. 2018;2:1206–1217.
 48. Chew EY, Clemons TE, Agron E, et al. Ten-year follow-up of age-related macular degeneration in the age-related eye disease study: AREDS report no. 36. *JAMA Ophthalmol*. 2014;132:272–277.
 49. Pasupathy A, Connor CE. Population coding of shape in area V4. *Nature Neurosci*. 2002;5:1332–1338.
 50. Loffler G, Wilson HR, Wilkinson F. Local and global contributions to shape discrimination. *Vis Res*. 2003;43:519–530.
 51. Greferath U, Guymer RH, Vessey KA, Brassington K, Fletcher EL. Correlation of Histologic Features with In Vivo Imaging of Reticular Pseudodrusen. *Ophthalmology*. 2016;123:1320–1331.
 52. Chen L, Messinger JD, Zhang Y, Spaide RF, Freund KB, Curcio CA. subretinal drusenoid deposit in age-related macular degeneration: Histologic Insights Into Initiation, Progression to Atrophy, and Imaging. *Retina (Philadelphia, Pa)*. 2020;40:618–631.
 53. Lee SCS, Martin PR, Grunert U. Topography of Neurons in the Rod Pathway of Human Retina. *Invest Ophthalmol Vis Sci*. 2019;60:2848–2859.
 54. Jones BW, Kondo M, Terasaki H, Lin Y, McCall M, Marc RE. Retinal remodeling. *Japanese J Ophthalmol*. 2012;56:289–306.
 55. Khuu SK, Kalloniatis M. Spatial summation across the central visual field: implications for visual field testing. *J Vis*. 2015;15(1):15.1.16.
 56. Scheffrin BE, Bieber ML, McLean R, Werner JS. The area of complete scotopic spatial summation enlarges with age. *J Opt Soc Am A, Optics, Image Science, and Vision*. 1998;15:340–348.

57. Uddin D, Jeffrey BG, Flynn O, et al. Repeatability of Scotopic Sensitivity and Dark Adaptation Using a Medmont Dark-Adapted Chromatic Perimeter in Age-related Macular Degeneration. *Transl Vis Sci Technol.* 2020;9:31.
58. Machida S, Kondo M, Jamison JA, et al. P23H rhodopsin transgenic rat: correlation of retinal function with histopathology. *Invest Ophthalmol Vis Sci.* 2000;41:3200–3209.
59. Birch DG, Wen Y, Locke K, Hood DC. Rod sensitivity, cone sensitivity, and photoreceptor layer thickness in retinal degenerative diseases. *Invest Ophthalmol Vis Sci.* 2011;52:7141–7147.